Efficient generation of osteoclasts from human induced pluripotent stem cells and functional investigations of lethal *CLCN7*-related osteopetrosis

Uta Rössler, Anna Floriane Hennig, Nina Stelzer, Shroddha Bose, Johannes Kopp, Kent Søe, Lukas Cyganek, Giovanni Zifarelli, Salaheddine Ali, Maja von der Hagen, Elisabeth Tamara Strässler, Gabriele Hahn, Michael Pusch, Tobias Stauber, Zsuzsanna Izsvák, Manfred Gossen, Harald Stachelscheid, Uwe Kornak

Supplementary Methods

Reprogramming of hiPSCs

Human iPSC lines isWT1.13 and isWT1.14 (UMGi014-C clone 13 and 14) and human iPSC lines isWT7.21 and isWT7.22 (UMGi020-B clone 21 and 22) were generated from dermal fibroblasts from a healthy male donor and a healthy female donor, respectively, using the integration-free CytoTune-iPS 2.0 Sendai Reprogramming kit (Thermo Fisher Scientific) according to manufacturer's instructions with modifications, as described before.(1) Established iPSC lines were maintained in Matrigel-coated (growth factor reduced, BD Biosciences) plates, passaged every 4–6 days with Versene solution (Thermo Fisher Scientific) and cultured in StemMACS iPS-Brew XF medium (Miltenyi Biotec) supplemented with 2 µM Thiazovivin (Merck Millipore) on the first day after passaging with daily medium change for at least ten passages before being used for karyotyping and pluripotency characterization, according to methods as described in detail before.(1) Antibodies and primers used are listed in Table S11–13.

Global expression profiling

RNA was extracted from the cells and purified by using the Direct-zol™ RNA MiniPrep Kit (Zymo Research). Poly-A enrichment was conducted according to in-house protocols

And 50 million sequence reads per sample were generated on a HiSeq 1500 (Illumina) system. For RNAseq analysis FASTQ files were analyzed using our in-house pipeline. The files were quality controlled (FASTQC) adapters trimmed (BBMap) and mapped to GRCh37 (STAR). DESeq2 was used for differential gene expression analysis.[2] The heatmap analysis was performed using the R package ClustVis with hierarchical clustering by calculating all pairwise distances.[3] Objects with the smallest distance are merged in each step. Rows were centered and unit variance scaling applied to rows. The clustering was performed with correlation distances and average linkage. The sample to sample distances were generated with the function “dist()” of the R package DESeq2 that outputs a matrix with an overview of similarities and differences between samples. For statistical comparison ANOVA was used for a global p-value and a t-test performed using a pairwise comparison against all.

Supplementary References

1. Hanses U, Kleinsorge M, Roos L, Yigit G, Li Y, Barbarics B, et al. Intronic CRISPR Repair in a Preclinical Model of Noonan Syndrome-Associated Cardiomyopathy. Circulation. 2020;142(11):1059-1076.

2. Love MI, Huber W, Anders S. Moderated estimation of fold change and dispersion for RNA-seq data with DESeq2. Genome Biol. 2014;15(12):550.

3. Metsalu T, Vilo J. ClustVis: a web tool for visualizing clustering of multivariate data using Principal Component Analysis and heatmap. Nucleic Acids Res. 2015;43(W1):W566-70.

Supplementary Figures

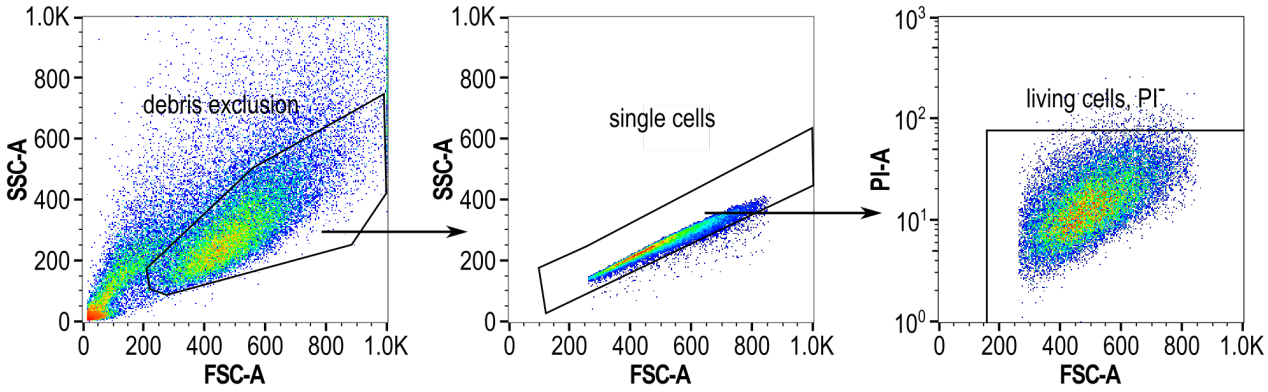

Supplementary Figure S1: **Gating strategy for flow cytometry.** Representative gating strategy for flow cytometry analysis to exclude cell debris, cell doublets and dead cells.

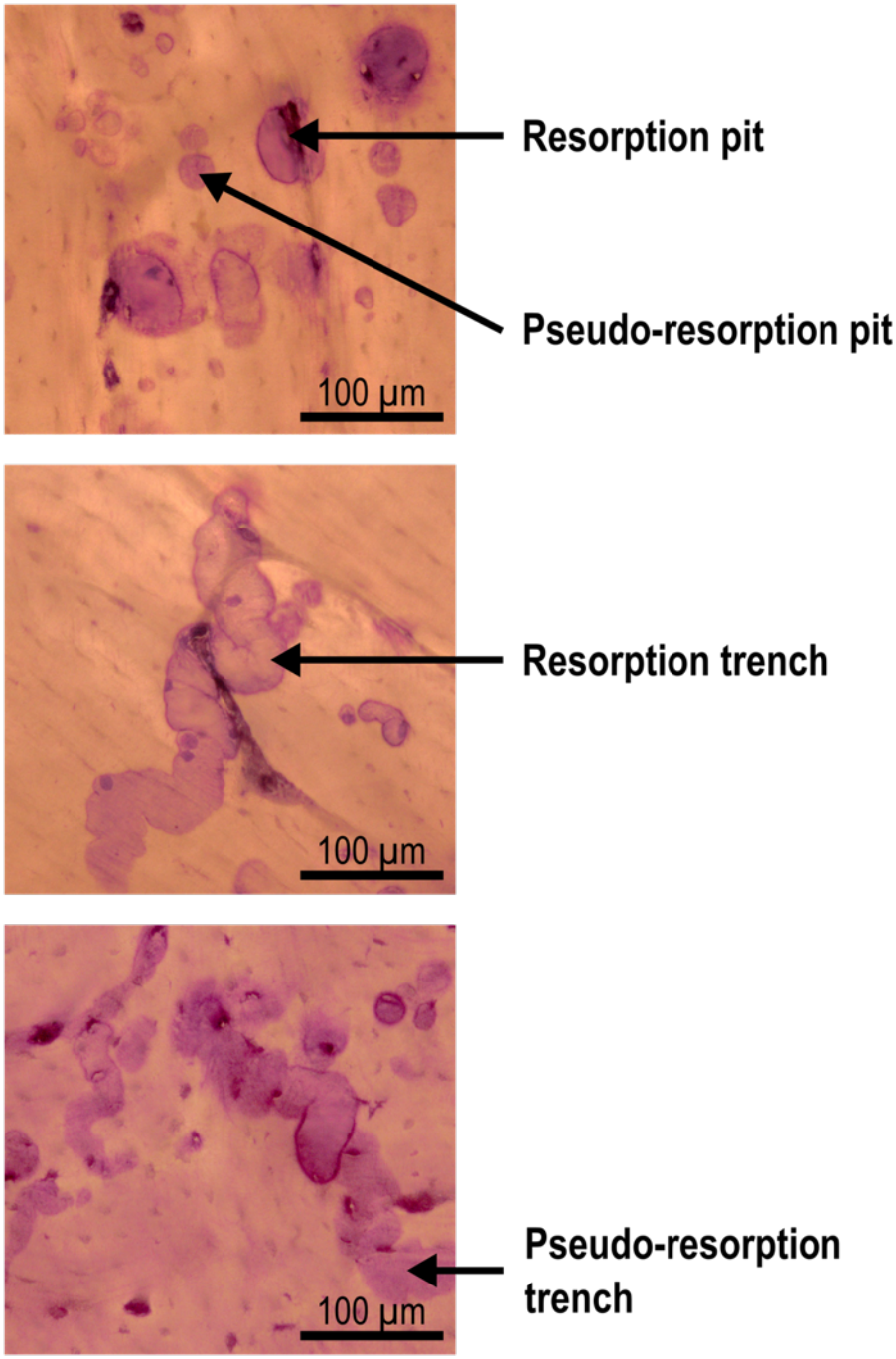

Supplementary Figure S2: Example pictures for different types of resorption. The osteoclast-mediated resorption on bovine cortical bone chips were classified according to the shape, depth and the presentation of the edges. Resorption pits were defined as excavation of round shape with well-defined edges and resorption trenches were identified by their elongated and continuous excavation shape with well-defined edges being at least two times longer than its width. Pseudo-resorption of both pits and trenches, were identified through careful analyses at the microscope by the lack of resorption depth (only staining) and therefore also have undefined edges.

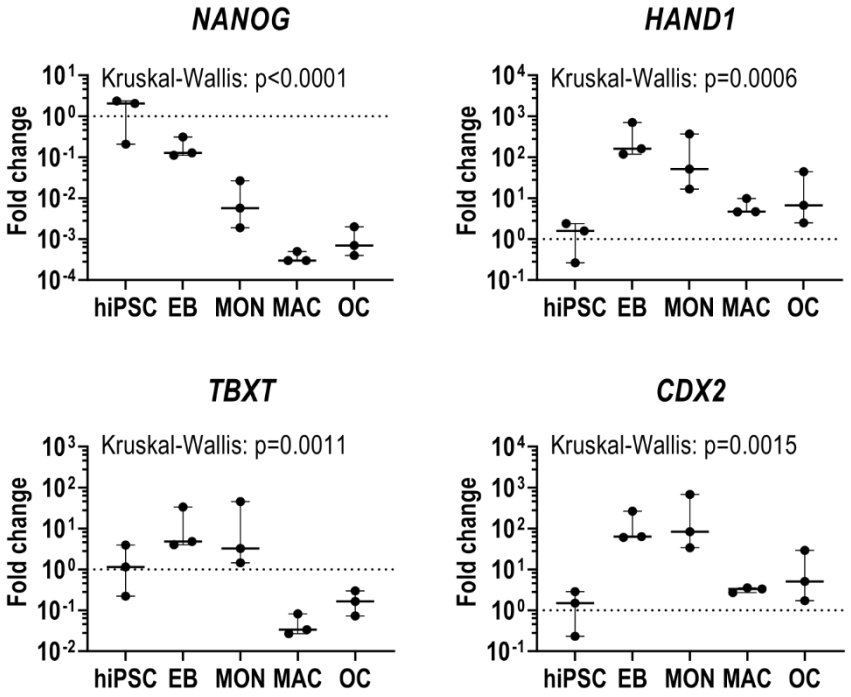

Supplementary Figure S3: Differentiation stage-specific gene expression in BIHi004-A hiPSC-derived cells. Expression of pluripotency marker *NANOG* and mesodermal markers *HAND1*, *TBXT* and *CDX2* in BIHi004-A hiPSC-derived cells determined by qRT-PCR analysis in undifferentiated hiPSCs, 4-day-old EBs, monocyte-like cells (MON), macrophages (MAC) and osteoclasts (OC). Relative mRNA expression is normalized to undifferentiated hiPSCs, *GAPDH* expression was used as housekeeping control. Data show boxplots with median, interquartile range, max and min values and all data points of three independent experiments. For statistical analysis, Kruskal-Wallis test and Dunn's multiple comparisons were used (Table S3).

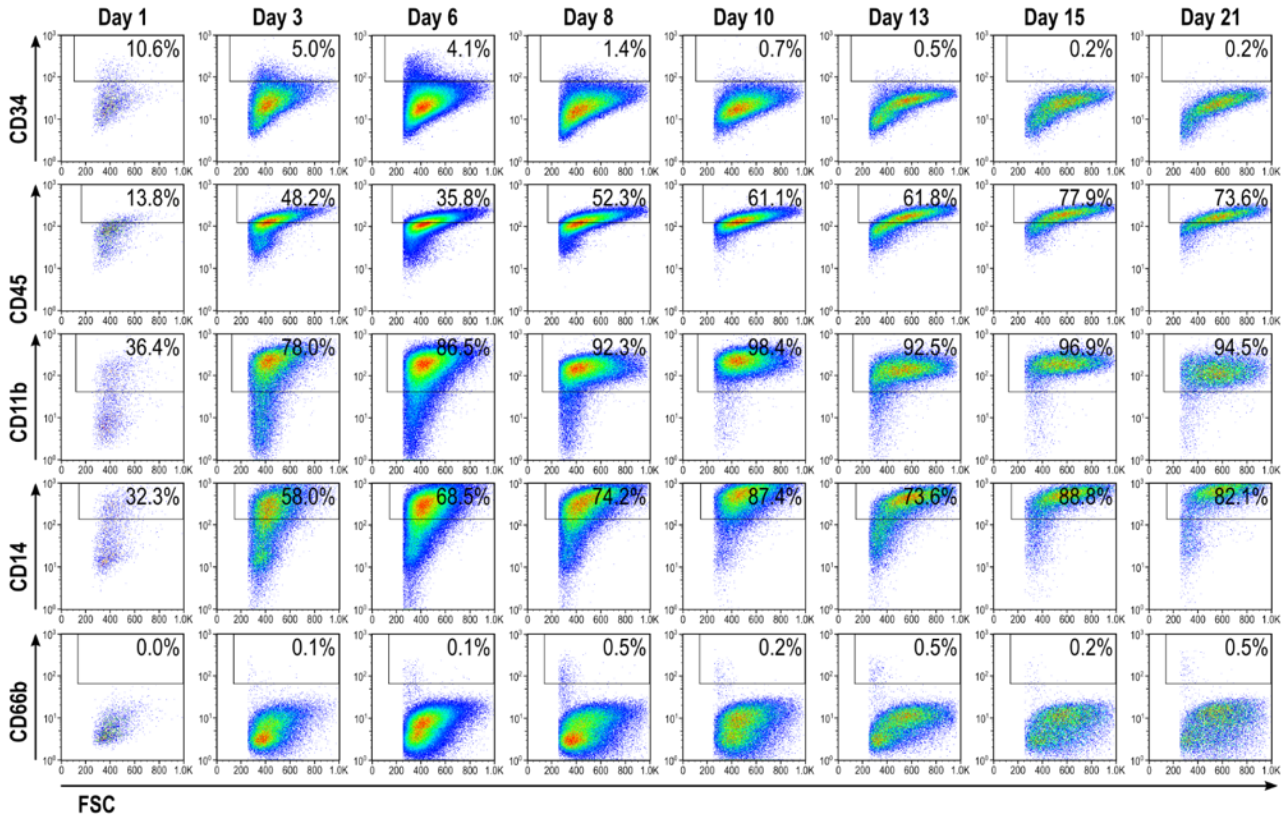

Supplementary Figure S4: Flow cytometry analysis of surface marker expression of monocyte-like cells of BIHi004-A hiPSCs over time. Gates show marker positive cells harvested and stained at different time points. Unstained and cells stained with isotype controls served as negative controls for gating (not shown).

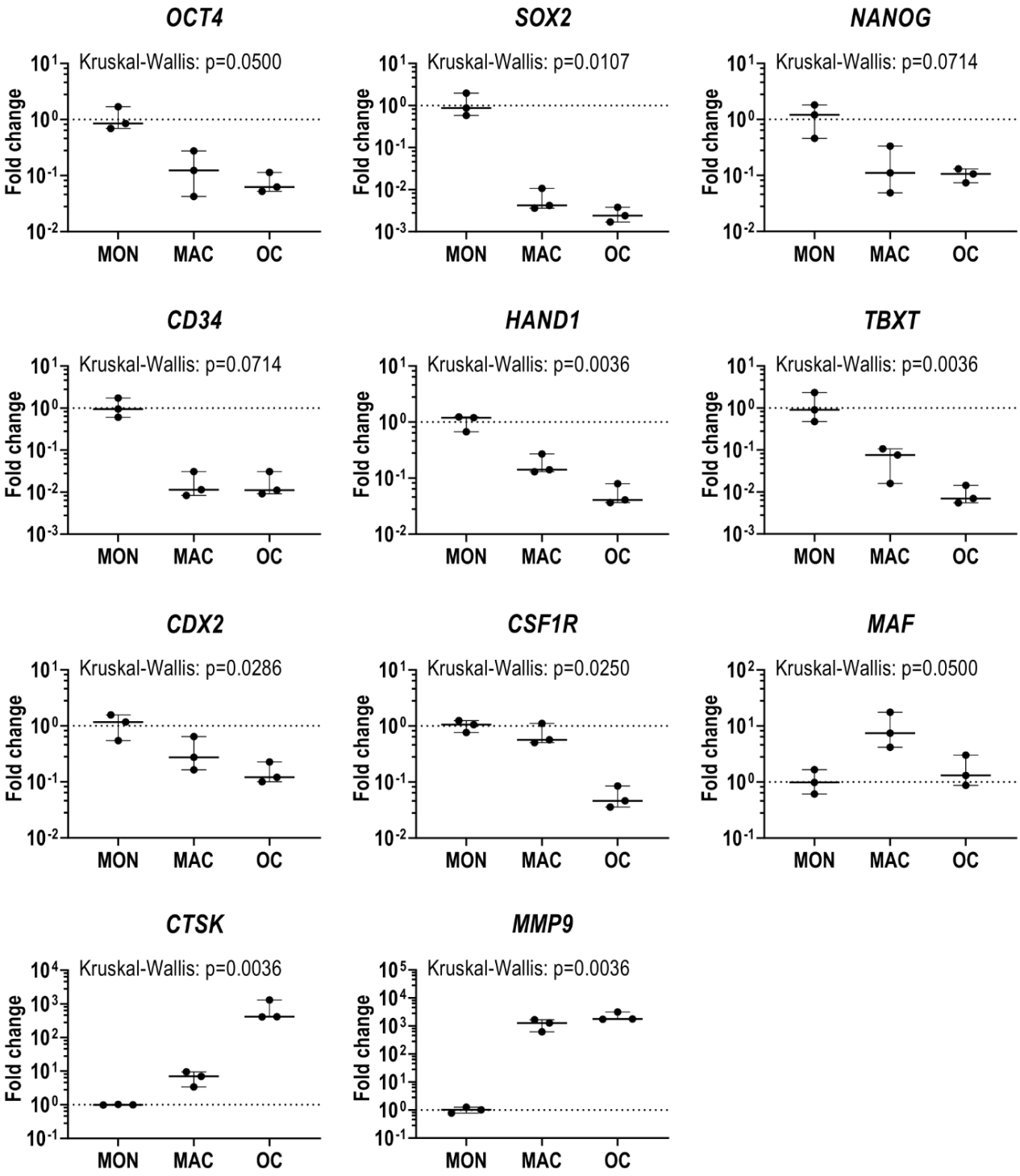

Supplementary Figure S5: Differentiation stage-specific gene expression in PBMC-derived osteoclasts. Expression of pluripotency markers *OCT4, SOX2* and *NANOG*, mesodermal markers *CD34*, *HAND1, TBXT* and *CDX2*, monocytic markers *CSF1R* and *MAF* and osteoclast markers *CTSK* and *MMP9* determined by qRT-PCR analysis in PBMC-derived monocytes (MON), macrophages (MAC), and osteoclasts (OC). Relative mRNA expression is normalized to monocytes, *GAPDH* expression was used as housekeeping control. Data show boxplots with median, interquartile range, max and min values and all data points of three independent experiments. For statistical analysis, Kruskal-Wallis test and Dunn's multiple comparisons were used (Table S5).

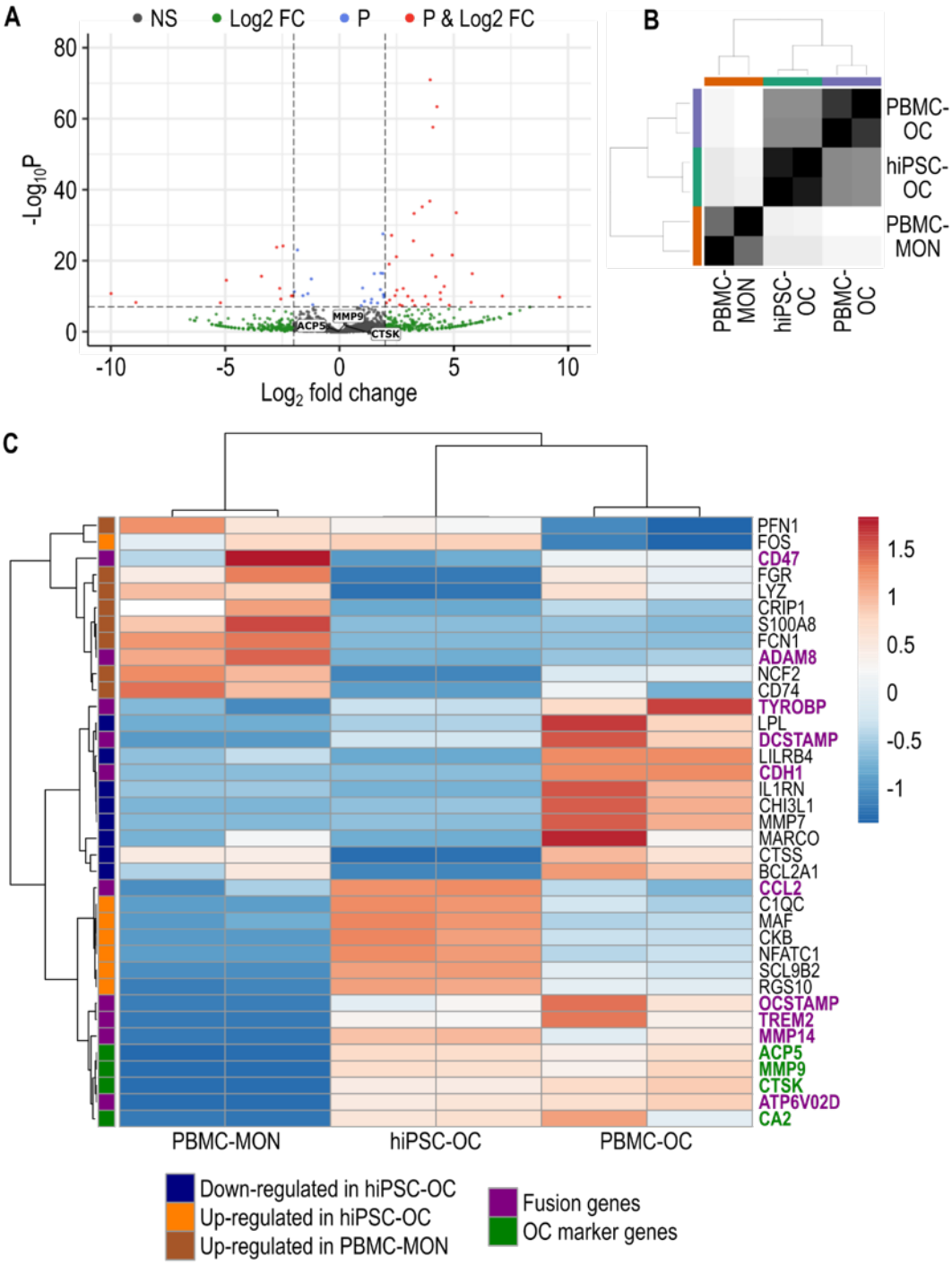

Supplementary Figure S6: Transcriptome comparison of PBMC-derived monocytes (PBMC-MON) and osteoclasts (PBMC-OC) with hiPSC-derived osteoclasts (hiPSC-OC)(n=2 for each group). **(A)** Volcano plot of expression comparison between PBMC- and hiPSC-derived osteoclasts. Values are given as -Log10 p-value over Log2 fold expression change. Black dots: no significant change (NS). Three non-significantly differentially expressed osteoclast marker genes are indicated. Green dots: ≥two-fold change, p-value >0.001 (Log2 FC), red dots: ≥two-fold change, p-value <0.001 (P & Log2 FC). **(B)** Sample distance matrix indicating the overall similarities of expression patterns. PBMC- and hiPSC-OC show close similarity, but are not identical. **(C)** heatmap of differentially expressed gene clusters. Note high similarity of PBMC- and hiPSC-derived osteoclasts and high expression of typical osteoclast marker genes (*ACP5, CA2, CTSK, MMP9*) in both cell types, but not in PBMC-monocytes. Most genes known to be involved in osteoclast fusion are more highly expressed in PBMC-OC. Note upregulation of *FOS, MAF*, and *NFATC1* in hiPSC-OC compared to PBMC-OC.

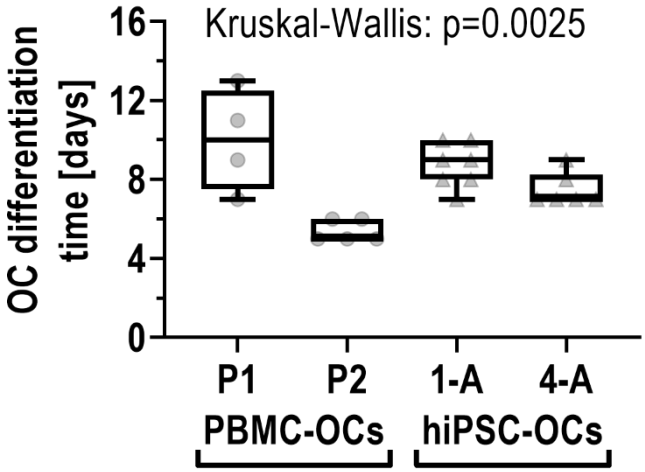

Supplementary Figure S7: Time-course analysis of osteoclast differentiation. Time was measured from seeding of monocytes until the development of the first visible osteoclasts. Monocytes from healthy PBMC donors P1 and P2 and control hiPSC lines BIHi001-A (1-A) and BIHi004-A (4-A) were used. Data show boxplots with median, interquartile range, max and min values and all data points of independent experiments. For statistical analysis, Kruskal-Wallis test and Dunn's multiple comparisons were performed (Table S7).

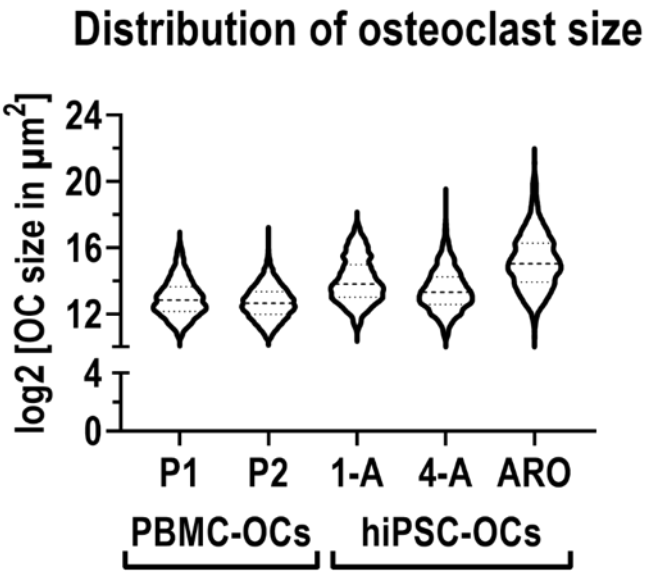

Supplementary Figure S8: Size of osteoclasts differentiated from PBMC- and hiPSC-derived monocytes. Log_2-transformed data from single osteoclasts measured in three independent pooled experiments are shown as violin plots with median and interquartile range. Cell size was determined in stained osteoclasts differentiated from healthy PBMC-donors P1 (n=2716) and P2 (n=4538) or the hiPSC-lines BIHi001-A (1-A, n=1402), BIHi004-A (4-A, n=2893) and BIHi002-A (ARO, n=630).

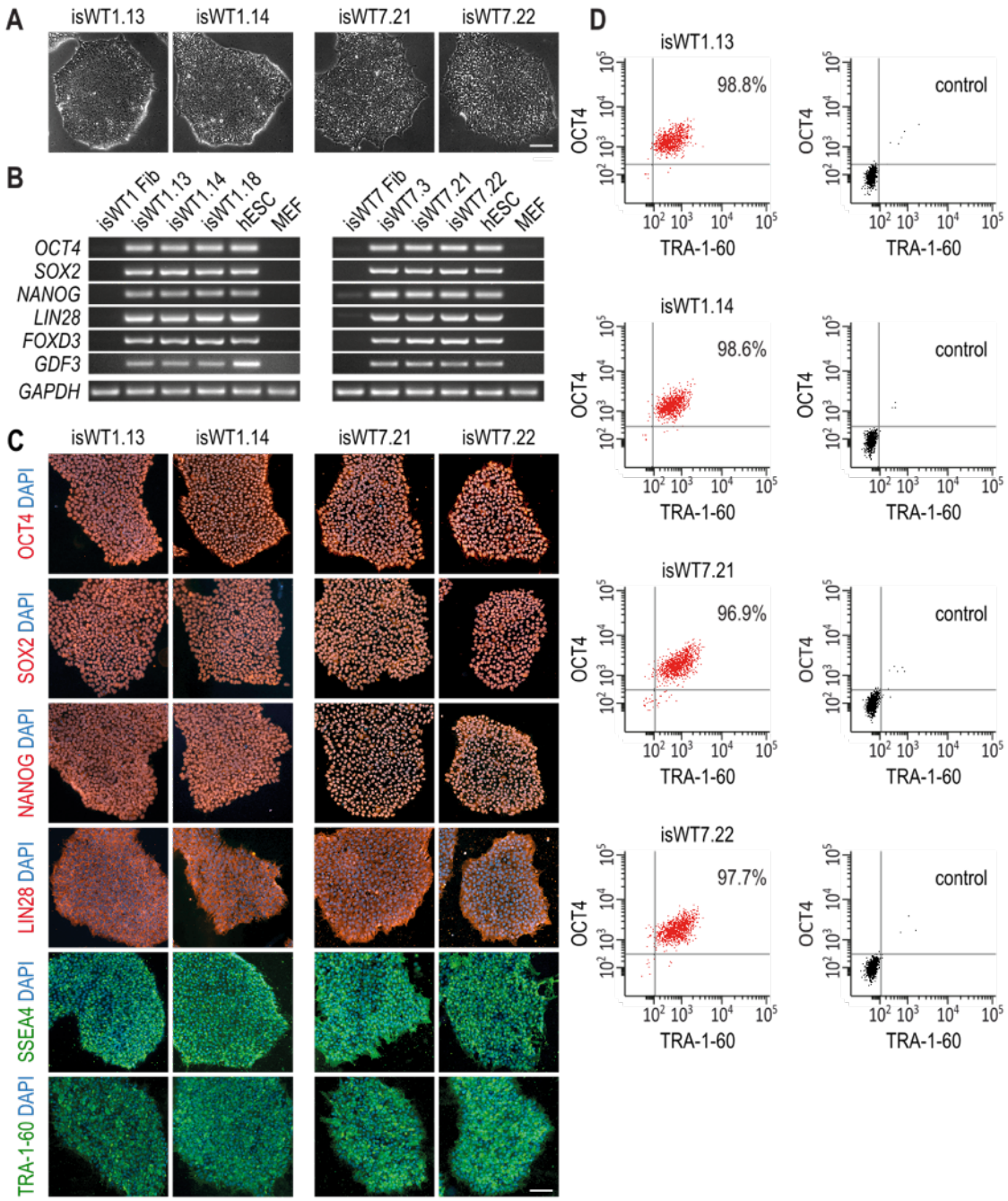

Supplementary Figure S9: Pluripotency characterization of human hiPSC lines isWT1 and isWT7. The hiPSC lines were reprogrammed from dermal fibroblasts from a healthy male (WT1) and a healthy female (WT7) donor by integration-free Sendai virus transduction. Two hiPSC lines per donor were selected for the experiments. **(A)** The generated hiPSC lines showed a typical human stem cell-like morphology. Scale bar: 100 µm. **(B)** Expression of endogenous pluripotency markers (*OCT4*, *SOX2*, *NANOG*, *LIN28*, *FOXD3*, *GDF3*) in hiPSC lines compared to donors' dermal fibroblasts was assessed by reverse transcriptase PCR; human embryonic stem cells (hESC) were used as positive control; mouse embryonic fibroblasts (MEF) were used as negative control. **(C)** Immunofluorescence staining for key pluripotency markers OCT4, SOX2, NANOG, LIN28 (all red), SSEA4 and TRA1-60 (both green) in the generated hiPSC lines. Nuclei were co-stained with DAPI (blue). Scale bar: 100 µm. **(D)** Flow cytometry analysis of pluripotency markers OCT4 and TRA-1-60 revealed homogeneous populations of pluripotent cells in generated hiPSC lines.

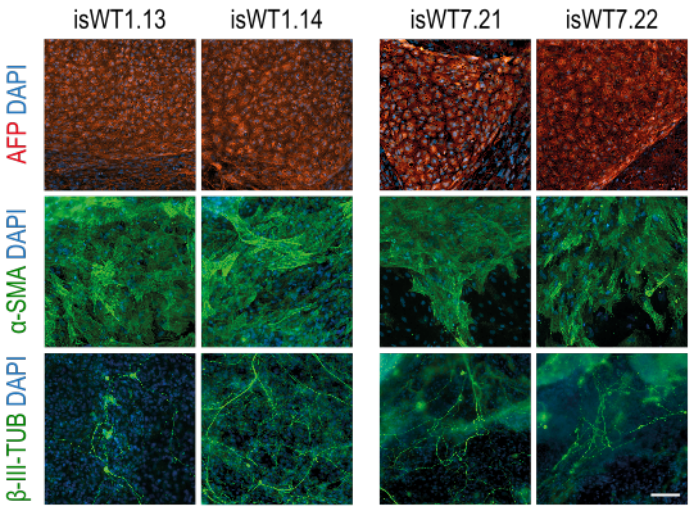

Supplementary Figure S10: Differentiation potential of generated isWT1 and isWT7 hiPSC lines. Spontaneous differentiation potential of generated iPSC lines was analyzed by embryoid body formation and germ-layer specific marker expression. Immunofluorescence staining of spontaneously differentiated hiPSC lines showed expression of endodermal marker AFP (red), mesodermal-specific α-SMA (green), and ectodermal β-III-tubulin (green). Nuclei were co-stained with DAPI (blue). Scale bar: 100 µm.

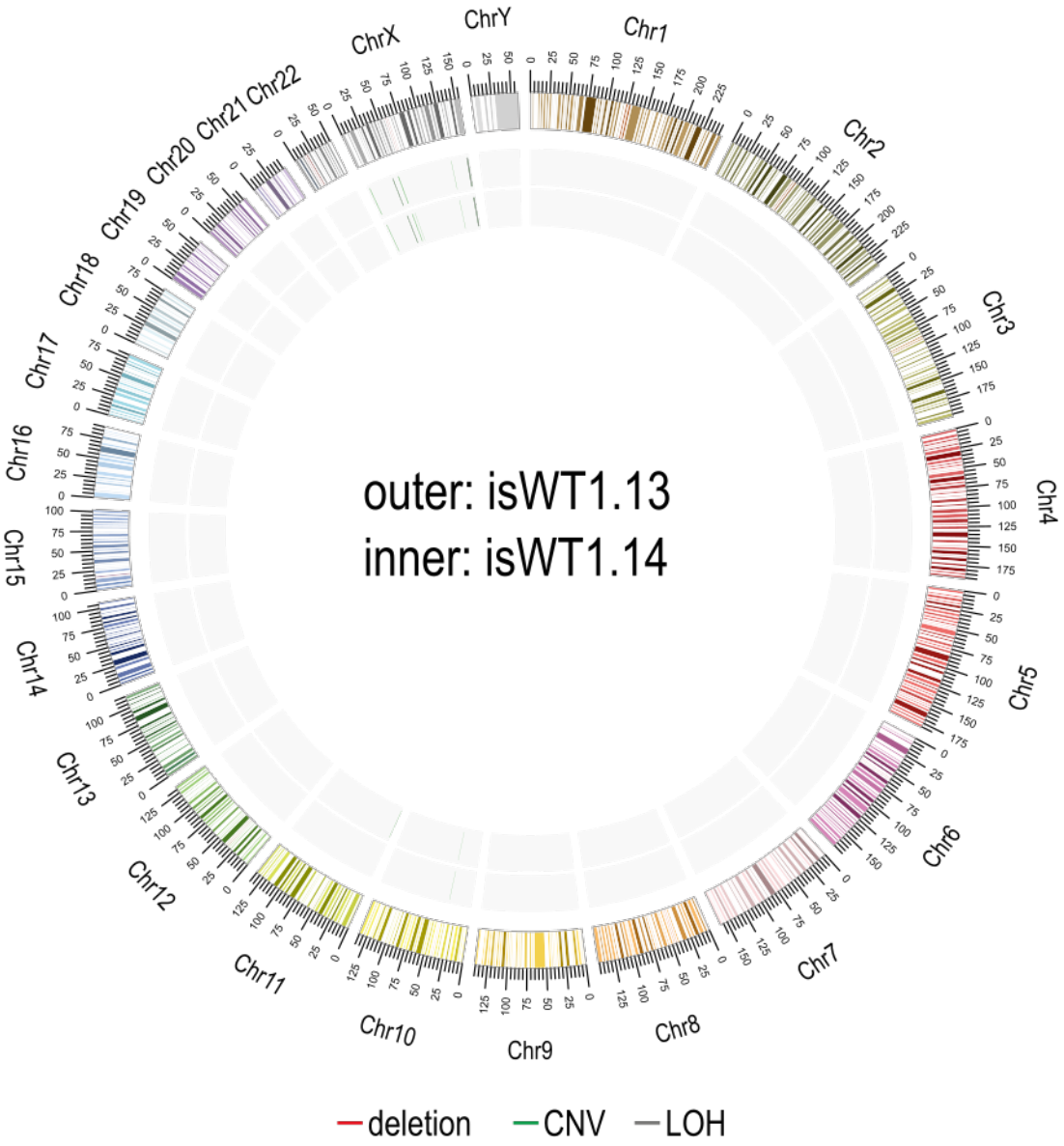

Supplementary Figure S11: Karyotype analysis of generated isWT1 hiPSC lines. Digital karyotypes of the hiPSC lines demonstrated chromosomal stability after transduction and passaging. Copy number variations (CNV) were reported if larger than 3.5×10^5 bps and 1×10^6 bps for loss of heterozygosity (LOH).

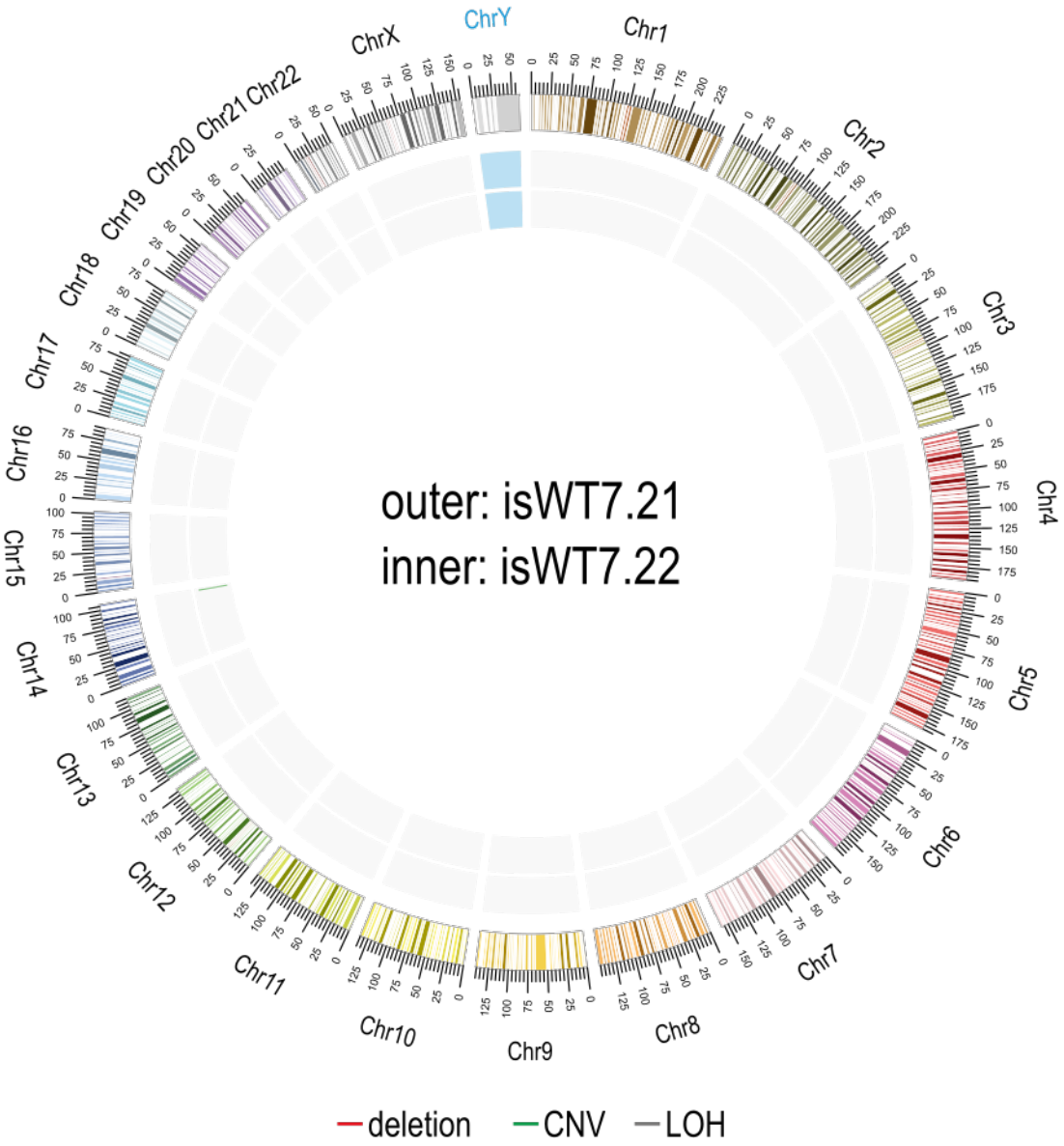

Supplementary Figure S12: Karyotype analysis of generated isWT7 hiPSC lines. Digital karyotypes of the hiPSC lines demonstrated chromosomal stability after transduction and passaging. Copy number variations (CNV) were reported if larger than 3.5×10^5 bps and 1×10^6 bps for loss of heterozygosity (LOH).

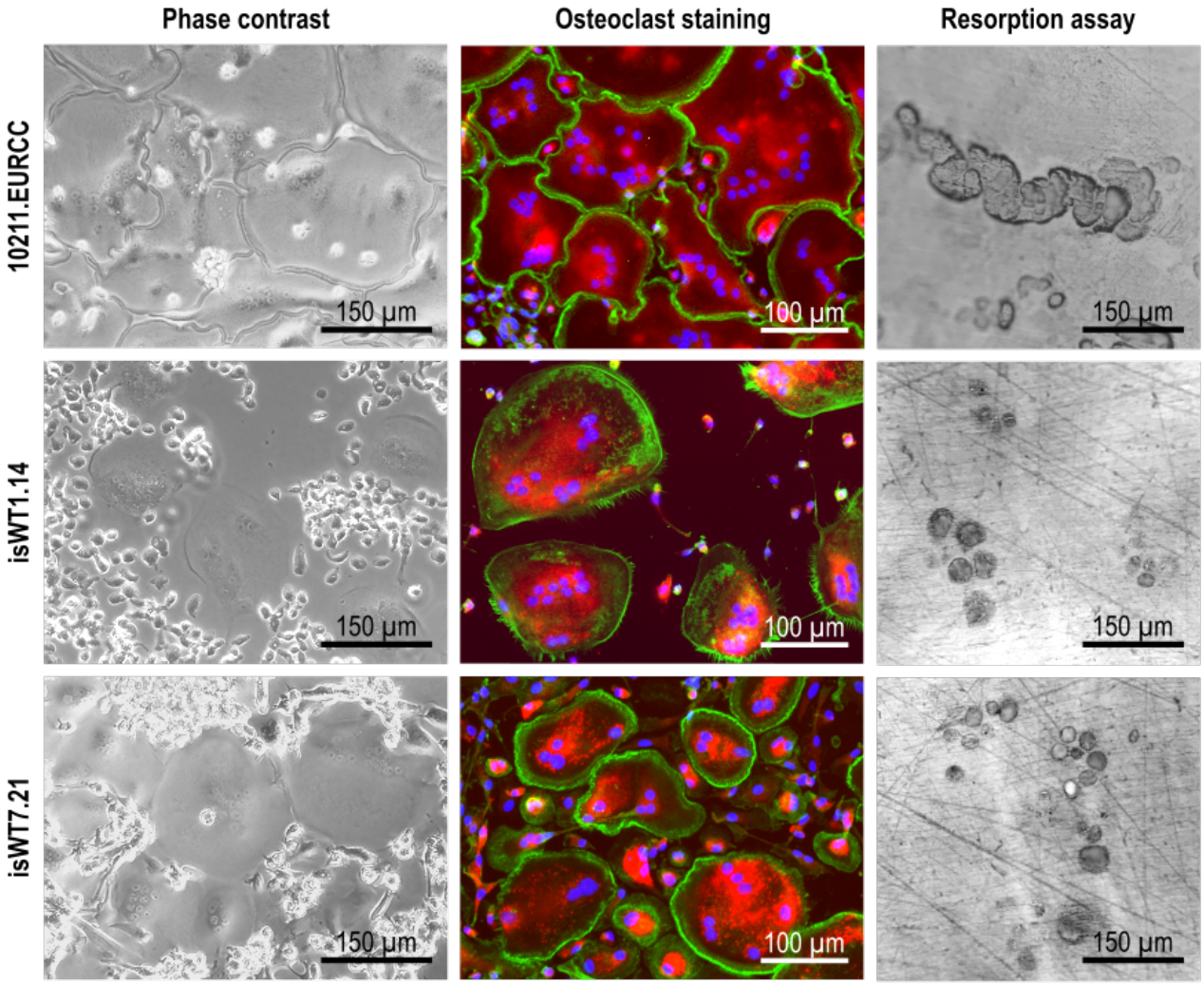

Supplementary Figure S13: Osteoclast differentiation of control hiPSCs. Functional osteoclasts were differentiated out of control hiPSC lines 10211.EURCC, isWT1.14 and isWT7.21 derived from healthy donors. Shown are representative images of osteoclasts in culture (phase contrast), stained osteoclasts (Phalloidin in green, TRAcP in red, DAPI in blue) and osteoclast-mediated resorption shown as black stained cavities on dentine.

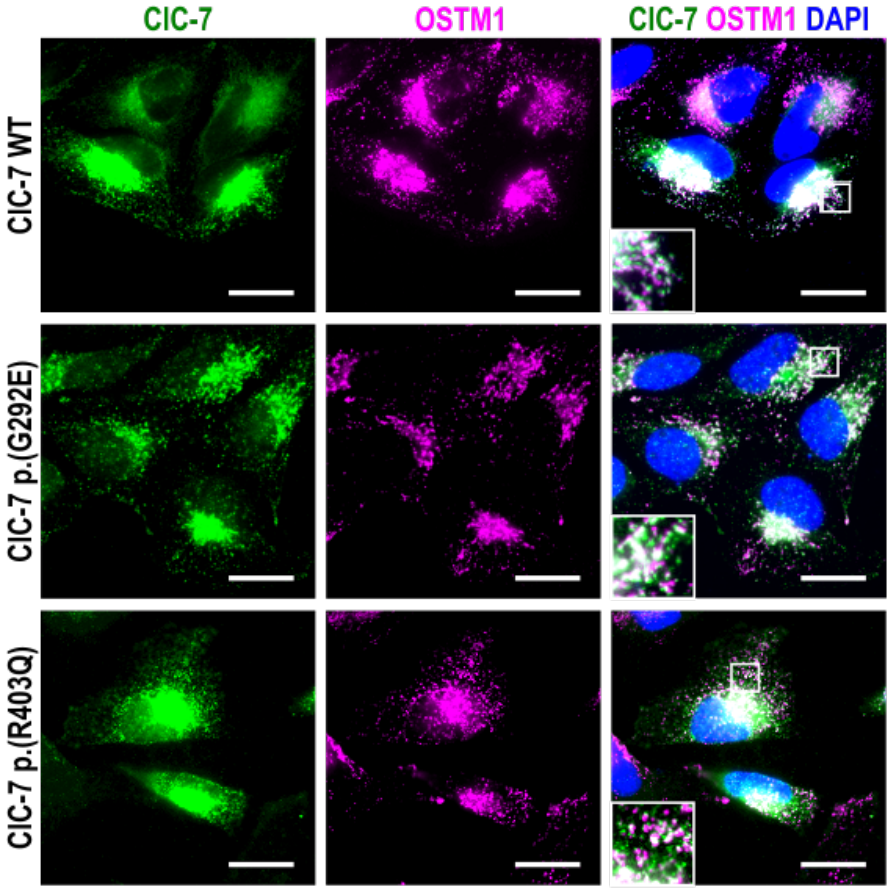

Supplementary Figure S14: Co-localization of ClC-7 and OSTM1. Co-localization of ClC-7 and OSTM1 in HeLa cells transfected with OSTM1-RFP and either WT or mutated hClC-7 shown by immunostaining: anti-ClC-7 (green), OSTM1-RFP (pink), DAPI (blue). Scale bar represents 25 µm.

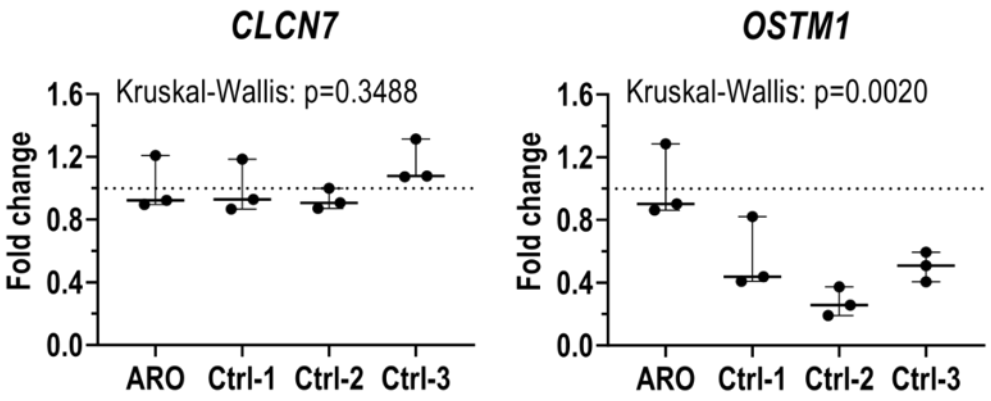

Supplementary Figure S15: *CLCN7* and *OSTM1* gene expression in control and patient ARO hiPSCs. Relative mRNA expression is normalized to ARO hiPSCs, *GAPDH* expression was used as housekeeping control. RNA was taken from undifferentiated ARO hiPSCs (BIHi002-A) and the three control hiPSC lines isWT1 (Ctrl-1), isWT7 (Ctrl-2) and BIHi001-A (Ctrl-3). Data show boxplots with median, interquartile range, max and min values and all data points of three independent experiments. For statistical analysis, Kruskal-Wallis test and Dunn's multiple comparisons were used (Table S9).

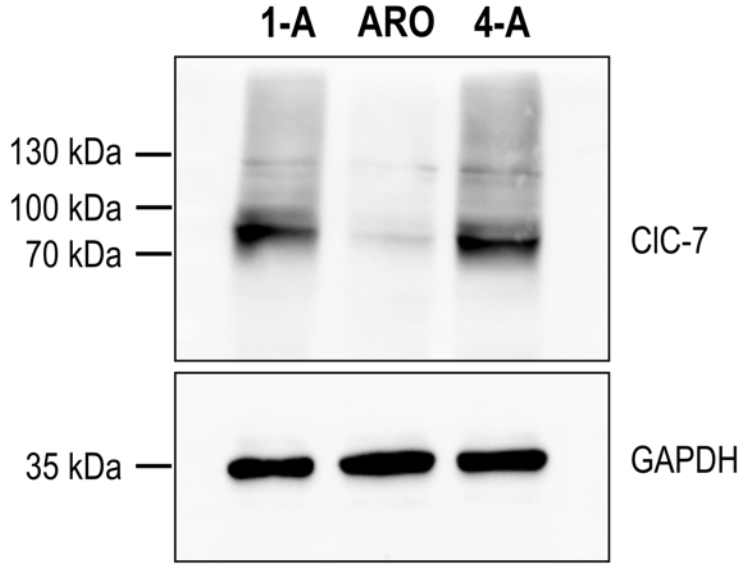

Supplementary Figure S16: ClC-7 western blot analysis. Representative ClC-7 immunoblot of control hiPSCs BIHi001-A (1-A) and BIHi004-A (4-A) and ARO hiPSCs.

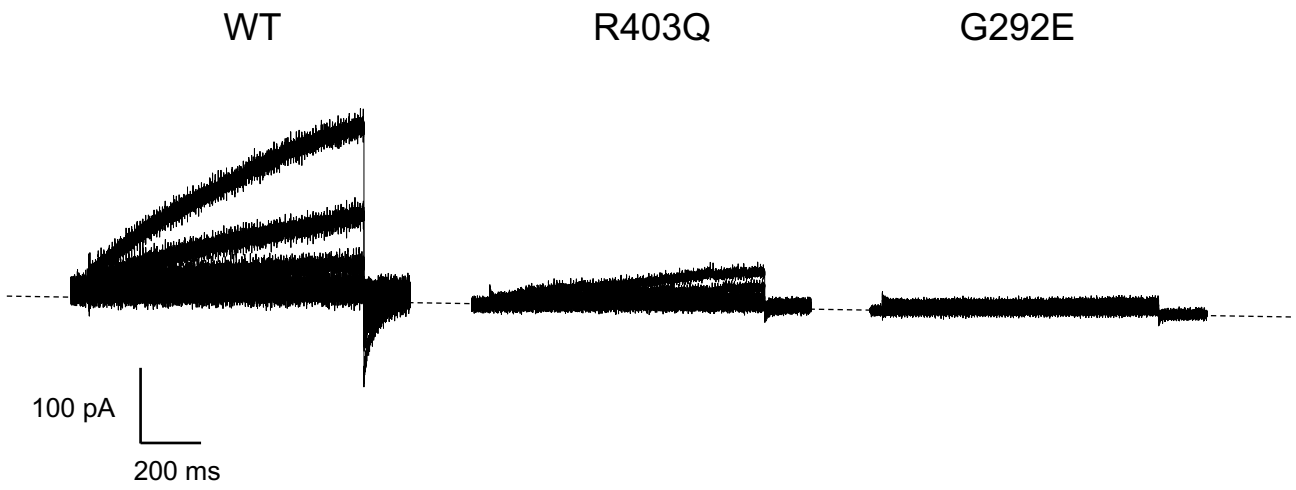

Supplementary Figure S17: Representative current traces of ClC-7 electrophysiology analysis. Currents were measured in HEK-293 cells expressing WT, p.(G292E) and p.(R403Q) ClC-7.

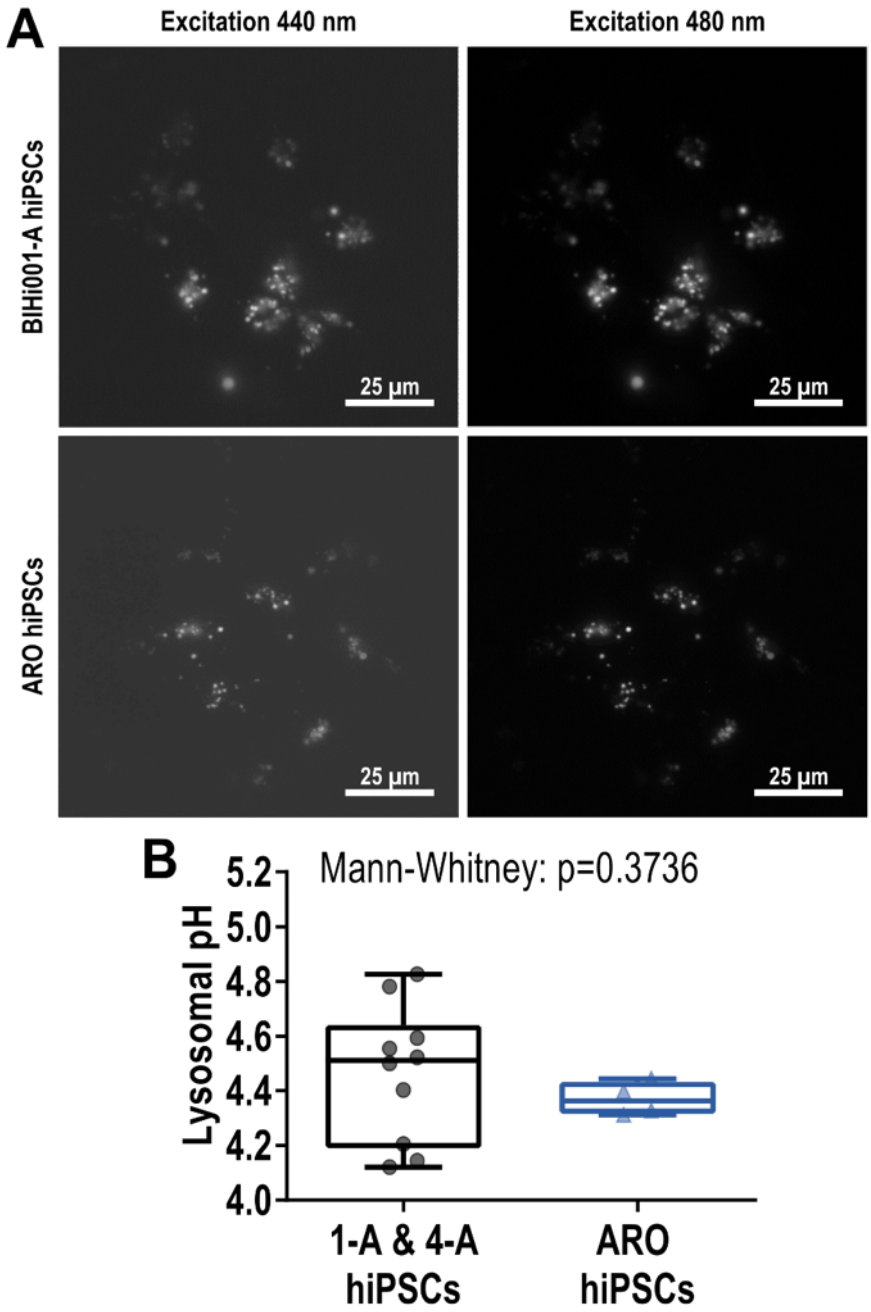

Supplementary Figure S18: Lysosomal pH measurement. (A) Representative images of pH measurements. In BIHi001-A and ARO hiPSCs lysosomes were loaded with Oregon Green 488-dextran for ratiometric pH measurement. Images were acquired using a Leica DMi8 microscope (Leica Microsystems). After determination of a calibration curve, the resulting fluorescence intensity ratio (488/440) as a function of pH was fit to a sigmoid and used to interpolate pH values from the experimental ratio data. **(B)** Quantification of lysosomal pH measurements. Shown are pooled data of three independent experiments as boxplots with median, interquartile range, max and min values and all data points. Significance was calculated by Mann-Whitney test (control hiPSCs 1-A and 4-A n=10, ARO hiPSCs n=4).

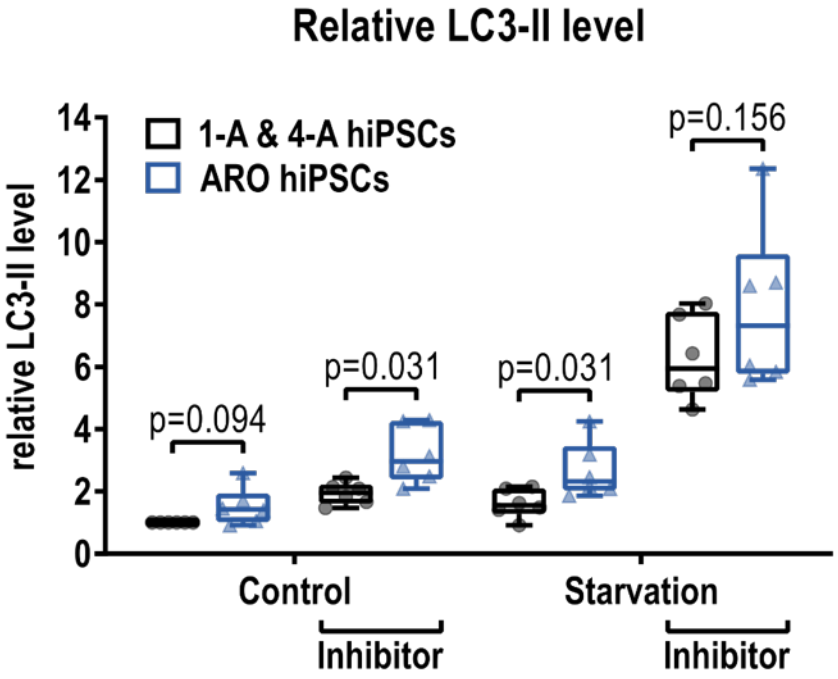

Supplementary Figure S19: Protein expression levels of autophagy marker LC3-II in undifferentiated control and ARO hiPSCs. Densitometric quantification of relative LC3-II levels of BIHi001-A (1-A), BIHi004-A (4-A) and ARO hiPSCs in control culture conditions or starvation with or without autophagy inhibitor (representative western blot shown in Figure 5). Shown are boxplots with median, interquartile range, max and min values and all pooled data points of three independent experiments (n=6). LC3-II levels were quantified against the loading control GAPDH and normalized to BIHi001-A and BIHi004-A in control culture conditions. Significance was calculated by Wilcoxon matched-pairs signed rank test.

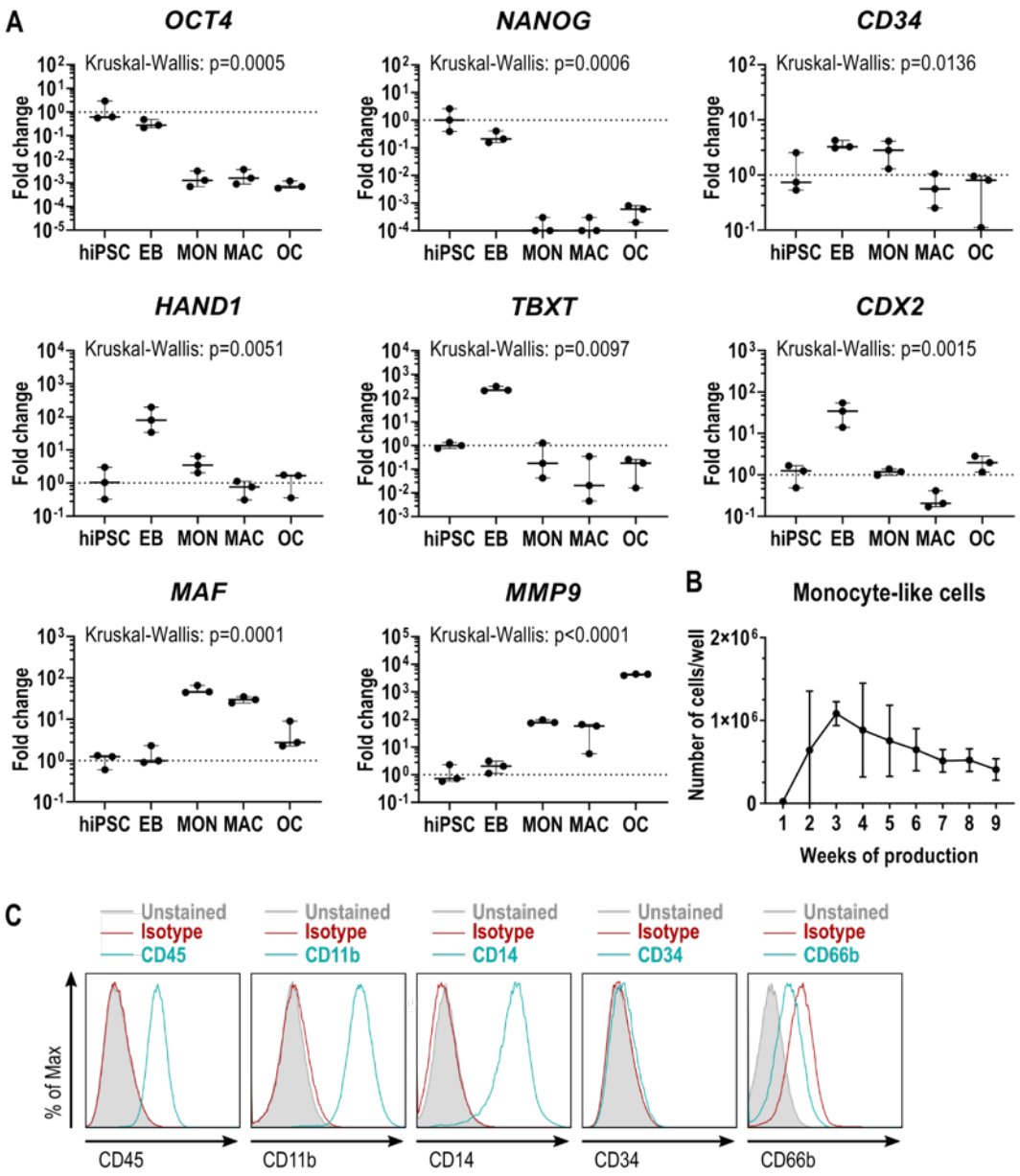

Supplementary Figure S20: Analysis of ARO hiPSC-derived cells at different stages of osteoclast differentiation. (A) Expression of pluripotency markers *OCT4* and *NANOG*, mesodermal markers *CD34, HAND1, TBXT* and *CDX2*, monocytic marker *MAF* and osteoclast marker *MMP9* determined by qRT-PCR analysis in ARO hiPSC-derived cells in undifferentiated hiPSCs, 4-day-old EBs, monocyte-like cells (MON), macrophages (MAC) and osteoclasts (OC). Relative mRNA expression is normalized to undifferentiated hiPSCs, *GAPDH* expression was used as housekeeping control. Data show boxplots with median, interquartile range, max and min values and all data points of three independent experiments. For statistical analysis, Kruskal-Wallis test and Dunn's multiple comparisons were used (Table S10). **(B)** Kinetics of monocyte-like cell production in ARO hiPSCs. Data are absolute numbers of harvested suspension cells per 6-well containing 8 myeloid cell forming complexes (means ± SD of three independent experiments, each with 12 6-wells). **(C)** Representative flow cytometry analysis of monocyte-like cells (harvested in week 5 after EB transfer) of ARO hiPSCs. Histograms show unstained cells (grey filled), cells stained with isotype controls (red) and cells stained with surface markers (blue).

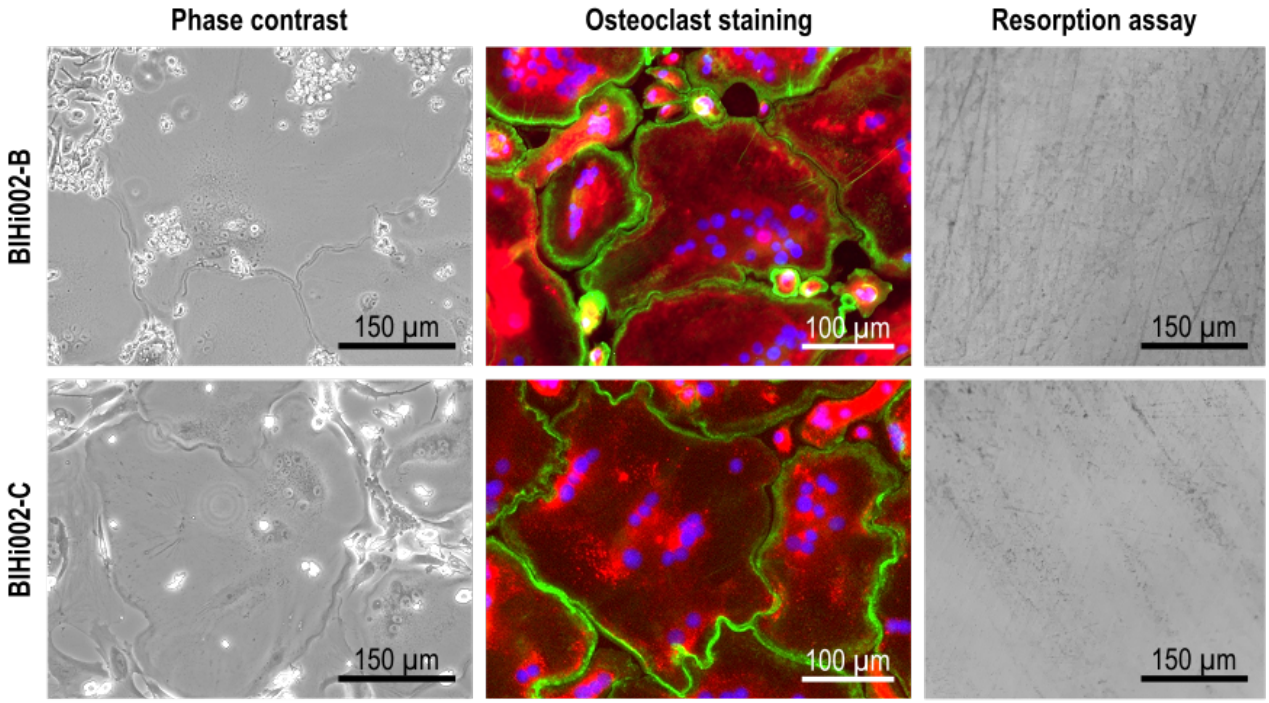

Supplementary Figure S21: Osteoclast differentiation of ARO hiPSCs. Osteoclast with lacking bone resorption activity were differentiated out of ARO hiPSC lines BIHi002-B and BIHi002-C derived from an ARO patient (Figure 4). Shown are representative images of osteoclasts in culture (phase contrast), stained osteoclasts (Phalloidin in green, TRAcP in red, DAPI in blue) and lack of osteoclast-mediated resorption (resorption assay shows no black stained resorption cavities on dentine).

Supplementary Tables

Table S1: hiPSC lines.

hiPSC line	Donor	Reprogramming	Laboratory
BIHi001-A	Male (newborn), foreskin fibroblasts	Sendai-viral vectors (integration-free)	BIH Core Facility Stem Cells
BIHi004-A	Female (35-39 years), dermal fibroblasts	Episomal vectors (integration-free)	BIH Core Facility Stem Cells
BIHi002-A, BIHi002-B, BIHi002-C	Male ARO patient (1 year), PBMCs	Sendai viral vectors (integration-free)	BIH Core Facility Stem Cells
isWT1.13, isWT1.14	Male (31 years), dermal fibroblasts	Sendai-viral vectors (integration-free)	Stem Cell Unit UMG
isWT7.21, isWT7.22	Female (25 years), dermal fibroblasts	Sendai-viral vectors (integration-free)	Stem Cell Unit UMG
10211.EURCC	Female (53 years), dermal fibroblasts	Sendai-viral vectors (integration-free)	Prof. Aalto-Setälä, Tampere University

Table S2: qRT-PCR primers for osteoclast differentiation.

Target gene	Forward primer (5'–3')	Reverse primer (5'–3')
SOX2	GGGAAATGGGAGGGGTGCAAAAGAGG	TTGCGTGAGTGTGGATGGGATTGGTG
OCT4	GACAGGGGGAGGGAGGAGCTAGG	CTTCCCTCCAACCAGTTGCCCCAAAC
NANOG	CAGCCCCGATTCTTCCACCAGTCCC	CGGAAGATTCCCAGTCGGGTTCACC
HAND1	GAAAGCAAGCGGAAAAGGGAG	GGTGCGCCCTTTAATCCTCTT
CD34	AAATCCTCTTCCTCTGAGGCTGGA	AAGAGGCAGCTGGTGATAAGGGTT
TBXT	TGTCCCAGGTGGCTTACAGATGAA	GGTGTGCCAAAGTTGCCAATACAC
CDX2	CCCTAGGAAGCCAAGTGAAAACC	CTCCTTGGCTCTGCGGTTCTG
CSF1R	TCCAACATGCCGGCAACTA	GCTCAAGTTCAAGTAGGCACTCTCT
MAF	GTACAAGGAGAAATACGAGAAG	TATGAAAAACTCGGGAGAGG
CTSK	CCACGTGGAGCTATGGAAGA	GCCTCAAGGTTATGGATGGA
MMP9	GCAGTACCACGGCCAACTA	GCCTTGGAAGATGAATGGAA
CLCN7	AGCAACGTGACCTACGGCTT	CATGTCGTACAGGCCCTCAAT
OSTM1	CCTTGCAGTGACACAGTGCCT	TGGACTTGAGACGTTTGGGCAG
GAPDH	CCATGTTCGTCATGGGTGTGAAC	CGGCCATCACGCCACAGTTT

Table S3: Statistical analysis of qRT-PCRs with BIHi004-A hiPSC-derived cells.

Specification	p-value
Dunn's multiple comparisons, Fig. 1*B* (*OCT4*)	
hiPSC vs. EB	>0.9999
hiPSC vs. MON	0.3965
hiPSC vs. MAC	0.0039
hiPSC vs. OC	0.0535
Dunn's multiple comparisons, Fig. 1*B* (*SOX2*)	
hiPSC vs. EB	0.7330
hiPSC vs. MON	0.7953
hiPSC vs. MAC	0.0053
hiPSC vs. OC	0.0600
Dunn's multiple comparisons, Fig. 1*B* (*CD34*)	
EB vs. hiPSC	0.4014
EB vs. MON	0.9413
EB vs. MAC	0.0056
EB vs. OC	0.1138
Dunn's multiple comparisons, Fig. 2*C* (*CSF1R*)	
MON vs. hiPSC	0.0548
MON vs. EB	0.4014
MON vs. MAC	>0.9999
MON vs. OC	>0.9999
Dunn's multiple comparisons, Fig. 2*C* (*MAF*)	
MON vs. hiPSC	0.0139
MON vs. EB	0.0186
MON vs. MAC	>0.9999
MON vs. OC	0.4014
Dunn's multiple comparisons, Fig. 3*B* (*CTSK*)	
OC vs. hiPSC	>0.9999
OC vs. EB	0.6836
OC vs. MON	0.0041
OC vs. MAC	0.0548
Dunn's multiple comparisons, Fig. 3*B* (*MMP9*)	
OC vs. hiPSC	0.0899
OC vs. EB	0.4014
OC vs. MON	0.8050
OC vs. MAC	0.0104
Dunn's multiple comparisons, Fig. S3 (*NANOG*)	
hiPSC vs. EB	>0.9999
hiPSC vs. MON	0.4002
hiPSC vs. MAC	0.0076
hiPSC vs. OC	0.0701
Dunn's multiple comparisons, Fig. S3 (*HAND1*)	
EB vs. hiPSC	0.0076
EB vs. MON	>0.9999
EB vs. MAC	0.2209
EB vs. OC	0.3313
Dunn's multiple comparisons, Fig. S3 (*TBXT*)	
EB vs. hiPSC	0.8050
EB vs. MON	>0.9999
EB vs. MAC	0.0139
EB vs. OC	0.1138
Dunn's multiple comparisons, Fig. S3 (*CDX2*)	
EB vs. hiPSC	0.0325
EB vs. MON	>0.9999
EB vs. MAC	0.2716
EB vs. OC	0.4828

Table S4: Frequency of living cells (PI-negative).

Day of analysis	PI-negative cells
Day 1	66.0 %
Day 3	88.8 %
Day 6	90.7 %
Day 8	91.8 %
Day 10	92.3 %
Day 13	90.0 %
Day 15	81.5 %
Day 21	85.2 %

Table S5: Statistical analysis of qRT-PCRs with monocyte-derived cells (donor P2).

Specification	p-value
Dunn's multiple comparisons, Fig. S5 (*OCT4*)	
MON vs. MAC	0.1473
MON vs. OC	0.0507
Dunn's multiple comparisons, Fig. S5 (*SOX2*)	
MON vs. MAC	0.2721
MON vs. OC	0.0225
Dunn's multiple comparisons, Fig. S5 (*NANOG*)	
MON vs. MAC	0.1053
MON vs. OC	0.0738
Dunn's multiple comparisons, Fig. S5 (*CD34*)	
MON vs. MAC	0.0738
MON vs. OC	0.1053
Dunn's multiple comparisons, Fig. S5 (*HAND1*)	
MON vs. MAC	0.3594
MON vs. OC	0.0146
Dunn's multiple comparisons, Fig. S5 (*TBXT*)	
MON vs. MAC	0.3594
MON vs. OC	0.0146
Dunn's multiple comparisons, Fig. S5 (*CDX2*)	
MON vs. MAC	0.4661
MON vs. OC	0.0341
Dunn's multiple comparisons, Fig. S5 (*CSF1R*)	
MON vs. MAC	0.9121
MON vs. OC	0.0341
Dunn's multiple comparisons, Fig. S5 *(MAF*)	
MON vs. MAC	0.0507
MON vs. OC	>0.9999
Dunn's multiple comparisons, Fig. S5 (*CTSK*)	
OC vs. MON	0.0146
OC vs. MAC	0.3594
Dunn's multiple comparisons, Fig. S5 (*MMP9*)	
OC vs. MON	0.0146
OC vs. MAC	0.3594

Table S6: Statistical analysis of osteoclast quantification.

Specification	p-value
Dunn's multiple comparisons, Fig. 3*C* (OC area*)*	
P1 vs. 1-A	>0.9999
P1 vs. 4-A	0.0150
P2 vs. 1-A	>0.9999
P2 vs. 4-A	0.4449
Dunn's multiple comparisons, Fig. 3*D* (OC size)	
P1 vs. 1-A	0.0009
P1 vs. 4-A	0.0619
P2 vs. 1-A	<0.0001
P2 vs. 4-A	<0.0001
Dunn's multiple comparisons, Fig. 3*D* (OC nuclei)	
P1 vs. 1-A	<0.0001
P1 vs. 4-A	<0.0001
P2 vs. 1-A	<0.0001
P2 vs. 4-A	0.0001
Dunn's multiple comparisons, Fig. 3*D* (OC density)	
P1 vs. 1-A	0.7554
P1 vs. 4-A	0.2280
P2 vs. 1-A	0.0007
P2 vs. 4-A	>0.9999

Table S7: Statistical analysis of osteoclast differentiation time-course.

Specification	p-value
Dunn's multiple comparisons, Fig. S7	
P1 vs. P2	0.0066
P1 vs. 1-A	>0.9999
P1 vs. 4-A	0.7194
P2 vs. 1-A	0.0066
P2 vs. 4-A	0.3005
1-A vs. 4-A	>0.9999

Table S8: Statistical analysis of bone resorption.

Specification	p-value
Dunn's multiple comparisons, Fig. 3*E* (eroded surface*)*	
P1 vs. 1-A	>0.9999
P1 vs. 4-A	0.4661
P2 vs. 1-A	0.3219
P2 vs. 4-A	0.0728
Dunn's multiple comparisons, Fig. 3*E* (trench frequency*)*	
P1 vs. 1-A	0.0910
P1 vs. 4-A	<0.0001
P2 vs. 1-A	0.0734
P2 vs. 4-A	<0.0001
Dunn's multiple comparisons, Fig. 3*E* (pseudo eroded surface*)*	
P1 vs. 1-A	0.4014
P1 vs. 4-A	0.9413
P2 vs. 1-A	0.0056
P2 vs. 4-A	0.1138

Table S9: Statistical analysis of hiPSC qRT-PCR.

Specification	p-value
Dunn's multiple comparisons, Fig. S15 (*CLCN7*)	
ARO vs. Ctrl-1	>0.9999
ARO vs. Ctrl-2	>0.9999
ARO vs. Ctrl-3	0.7726
Dunn's multiple comparisons, Fig. S15 (*OSTM1*)	
ARO vs. Ctrl-1	0.4231
ARO vs. Ctrl-2	0.0067
ARO vs. Ctrl-3	0.3388

Table S10: Statistical analysis of qRT-PCRs with BIHi002-A ARO hiPSC-derived cells.

Specification	p-value
Dunn's multiple comparisons, Fig. 6*A* (*SOX2*)	
hiPSC vs. EB	>0.9999
hiPSC vs. MON	0.1007
hiPSC vs. MAC	0.0103
hiPSC vs. OC	0.1271
Dunn's multiple comparisons, Fig. 6*A* (*CSF1R*)	
MON vs. hiPSC	0.0423
MON vs. EB	0.3313
MON vs. MAC	>0.9999
MON vs. OC	>0.9999
Dunn's multiple comparisons, Fig. 6*A* (*CTSK*)	
OC vs. hiPSC	0.0548
OC vs. EB	>0.9999
OC vs. MON	0.3313
OC vs. MAC	0.0056
Dunn's multiple comparisons, Fig. S20 (*OCT4)*	
hiPSC vs. EB	>0.9999
hiPSC vs. MON	0.0792
hiPSC vs. MAC	0.1777
hiPSC vs. OC	0.0088
Dunn's multiple comparisons, Fig. S202 (*NANOG*)	
hiPSC vs. EB	>0.9999
hiPSC vs. MON	0.0261
hiPSC vs. MAC	0.0261
hiPSC vs. OC	0.3193
Dunn's multiple comparisons, Fig. S20 (*CD34*)	
EB vs. hiPSC	0.1784
EB vs. MON	>0.9999
EB vs. MAC	0.0705
EB vs. OC	0.0705
Dunn's multiple comparisons, Fig. S20 (*HAND1*)	
EB vs. hiPSC	0.0899
EB vs. MON	>0.9999
EB vs. MAC	0.0186
EB vs. OC	0.1138
Dunn's multiple comparisons, Fig. S20 (*TBXT*)	
EB vs. hiPSC	>0.9999
EB vs. MON	0.1784
EB vs. MAC	0.0247
EB vs. OC	0.0548
Dunn's multiple comparisons, Fig. S20 (*CDX2*)	
EB vs. hiPSC	0.2716
EB vs. MON	0.2209
EB vs. MAC	0.0041
EB vs. OC	0.9413
Dunn's multiple comparisons, Fig. S20 (*MAF*)	
MON vs. hiPSC	0.0139
MON vs. EB	0.0247
MON vs. MAC	>0.9999
MON vs. OC	0.3313
Dunn's multiple comparisons, Fig. S20 (*MMP9*)	
OC vs. hiPSC	0.0076
OC vs. EB	0.0325
OC vs. MON	>0.9999
OC vs. MAC	0.4014

Table S11: Primary antibodies for hiPSC reprogramming.

Primary antibody	Supplier	Catalog Number (Research Resource Identifier)
AFP polyclonal rabbit IgG	Dako	Cat# A0008 (RRID:AB_2650473)
α-SMA monoclonal mouse IgG2a	Sigma-Aldrich	Cat# A2547 (RRID:AB_476701)
β-III-tubulin monoclonal mouse IgG2a	Covance	Cat# MMS-435P (RRID:AB_2313773)
LIN28 polyclonal goat IgG	R and D Systems	Cat# AF3757 (RRID:AB_2234537)
NANOG polyclonal rabbit IgG	Thermo Fisher Scientific	Cat# PA1-097 (RRID:AB_2539867)
OCT3/4 polyclonal goat IgG	R and D Systems	Cat# AF1759 (RRID:AB_354975)
OCT3/4 conjugated Alexa Fluor 647 monoclonal mouse IgG1	BD Biosciences	Cat# 560329 (RRID:AB_1645318)
SOX2 monoclonal mouse IgG1	Thermo Fisher Scientific	Cat# MA1-014 (RRID:AB_2536667)
SSEA4 monoclonal mouse IgG3	Thermo Fisher Scientific	Cat# MA1-021 (RRID:AB_2536687)
TRA-1-60 monoclonal mouse IgM	Abcam	Cat# ab16288 (RRID:AB_778563)
TRA-1-60 conjugated Alexa Fluor 488 monoclonal mouse IgM	BD Biosciences	Cat# 560173 (RRID:AB_1645379)

Table S12: Secondary antibodies for hiPSC reprogramming.

Secondary antibody	Supplier	Catalog Number (Research Resource Identifier)
Alexa Fluor 488 polyclonal donkey anti-mouse IgG	Thermo Fisher Scientific	Cat# A-21202 (RRID:AB_141607)
Alexa Fluor 555 polyclonal donkey anti-goat IgG	Thermo Fisher Scientific	Cat# A-21432 (RRID:AB_2535853)
Alexa Fluor 555 polyclonal donkey anti-mouse IgG	Thermo Fisher Scientific	Cat# A-31570 (RRID:AB_2536180)
Alexa Fluor 555 polyclonal donkey anti-rabbit IgG	Thermo Fisher Scientific	Cat# A-31572 (RRID:AB_162543)
FITC polyclonal goat anti-mouse IgM	Jackson ImmunoResearch Labs	Cat# 115-097-020 (RRID:AB_2338618)

Table S13: PCR primers for hiPSC repgramming.

Target gene	Forward primer (5'–3')	Reverse primer (5'–3')
FOXD3	GTGAAGCCGCCTTACTCGTAC	CGAAGCTCTGCATCATGAG
GDF3	TTCGCTTTCTCCCAGACCAAGGTTTC	TACATCCAGCAGGTTGAAGTGAACAGCACC
LIN28	AGTAAGCTGCACATGGAAGG	ATTGTGGCTCAATTCTGTGC
NANOG	AGTCCCAAAGGCAAACAACCCACTTC	ATCTGCTGGAGGCTGAGGTATTTCTGTCTC
OCT4	GACAACAATGAAAATCTTCAGGAGA	TTCTGGCGCCGGTTACAGAACCA
SOX2	ATGCACCGCTACGACGTGA	CTTTTGCACCCCTCCCATTT
GAPDH	AGAGGCAGGGATGATGTTCT	TCTGCTGATGCCCCCATGTT